Defence Science Journal, Vol. 57, No. 5, September 2007, pp. 677-690

Modelling of Shockwave Force and its Effect during Sabot Discard Process

R.S. Acharya[1] and S.D. Naik[2]

[1]*Vishwakarma Institute of Information Technology, Pune-411 048*
[2]*Defence Institute of Armament Technology, Pune-411 025*

ABSTRACT

The dynamical motion of a FSAPDS projectile is affected due to the propellant gas force, aerodynamic, gravity along with mechanical force, and shockwave forces. In the sabot opening process, the mechanical action takes place and the sabot gets separated due to the shockwave force. In external mechanical action of sabot separation, the maximum stretch of the spring defines the end of third phase of motion. In this paper the motion of the projectile and its stability during this phase has been presented. The time delay in the sabot opening affects the stability of the projectile is discussed with the help of modified stability parameter.

Keywords: Shockwave force, sabot discard process, FSAPDS projectile, dynamic motion, modelling

NOMENCLATURE

I_{xx}	Moment of inertia about the *X*-axis
I_{yy}	Moment of inertia about the *Y*-axis
I_{zz}	Moment of inertia about the *Z*-axis
m	Mass
C	Mass centre of projectile sabot
C_i	Mass center of the projectile sabot
r	Position vector
V	Velocity
A	Projectile reference area
O-XYZ	Inertial coordinate system
P	Propellant gas pressure
P_2	Pressure at the tip of sabot
P_1	Pressure at opening of sabot
γ	Specific heat ratio
M	Shock Mack number
a	Velocity of sound
$O1i$	Tip of the sabot
ρ	Air density
ρ_s	Density of the gas in the vicinity of sabot
P	Pressure in gas flow
l	Projectile characteristics length
x, y, z	Range, altitude, and drift, respectively
$C_{L\alpha}$ /$C_{N\alpha}$	Lift/Normal coefficient
C_D /C_X	Drag/Axial coefficient
F_1/M_1	Propellant gas force/moment
F_2/M_2	Aerodynamic force/moment
F_3/M_3	Gravity force/moment
$C_{M\alpha}$	Overturning moment
$C_{Mp\alpha}$	Magnus moment coefficient
$C_{Np\alpha}$	Magnus force coefficient

Received 2 January 2006, revised 7 September 2006

C_{Mqt}	Pitch damping moment coefficient
C_{Nqt}	Pitch damping force coefficient
u, v, w	Velocity components in projectile frame
$\omega_1,\omega_2,\omega_3$	Angular velocity components of projectile
r_p	Position vector of the effective pressure point and centre of mass of the projectile
Ω	Angular velocity
δ_1,δ_2	Angles made by projectile axis in velocity frame
η_1,η_2	Angles made by the propellant gas direction in projectile frame
$\varepsilon_1,\varepsilon_2$	Angles made by propellant gas direction in inertial frame
p	Axial spin of the projectile
C_{tp}	Spin damping moment
C_v	Specific heat of gases around
Lc	Length between the centre and tip of sabot
Ls	Total length of the sabot
θ	Angle of attack
Φ	Angle of side slip

Convention

X	Vector cross product

Suffix

1	Denotes the projectile coordinate systems
2	Denotes the velocity coordinate systems
3	Denotes the sabot component fixed coordinate systems
p	Denotes the projectile component
s	Denotes the sabot component

1. INTRODUCTION

The motion of fin stabilised armor piercing discarding sabot (FSAPDS) is affected mainly by the forces acting during sabot discard process. Yang[1] has developed a theoretical model of the motion with three turning points and two transition periods (Fig.1). The first turning point is at the instant when the fixed circles of a sabot component reaches the limit stress state, and its groove teeth break at the same time due to the air dynamic force. The second turning point is at the instant when circle groove teeth of a sabot component separate from those of projectile body and their mechanical interaction vanishes also due to the air dynamic force. The moment is defined as the third turning point, when the intersect point between projectile and shock wave at the head of a sabot component moves to the projectile base, and the projectile is considered as getting from the influence region.

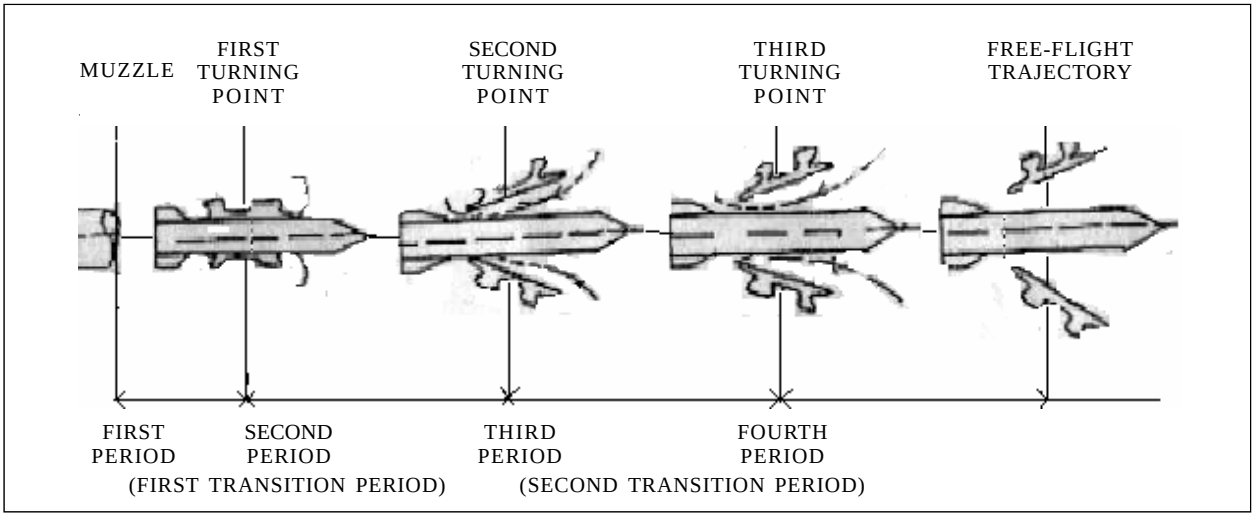

Figure 1. Turning points, four phases and transition periods of sabot discarding process.

The first phase is from the moment of the projectile leaving the gun muzzle to the first turning point. The second phase is from the first turning point to the second one. The third phase is between the second turning point and third one. The fourth phase is free flight phase of the projectile, during which the projectile gets rid of the sabot component influence.

For FSAPDS projectile, the trajectory and stability depend on different forces in different phases of the motion. The forces affecting the motion of the FSAPDS projectile are propellant gas force, aerodynamic, gravity along with mechanical force and shockwave forces. Here, the aerodynamics forces considered are: Drag force, lift force, magnus force, and pitch damping force. During the first phase[2] the gravity, aerodynamics forces along with propellant gas force affect the motion. The motion is influenced by shockwave and mechanical force during sabot opening, which was discussed in the second phase [3]. Due to mechanical as well as shockwave forces, the sabot starts separating from the projectile. The small angle θ_{3i} is developed between the sabot and the projectile (Fig. 2).

In the third phase, the gas flow enters between the projectile body and the sabot, pressure increases impulsively and the area of the cross section at the tip of sabot increases. At a particular instant, the area is sufficiently increased that, the sabot gets totally separated from the projectile.

Different aspects of saboted projectile study have been studied since 1957. Gallagher[4] presented an experimental design of projectile deviation from the desired aim point due to muzzle blast, sabot discard, and projectile asymmetry. Conn[5] investigated the effect of aerodynamic interference between sabots and projectiles fired from a light gas gun on conical projectile launched with a two-segment sabot. Schmist and Shear[6] investigated the trajectory disturbances originating during the discard of sabot components from gun-launched fin-stabilized projectile. The motion of the projectile and separation sabot components were measured near the muzzle with flash x-rays. Siegelman and Crimi[7] used the experimental test data generated by BRL and developed an empirically-based model of the flow field around a projectile and its sabot components during discard and concluded that the flow field model coupled with a dynamic model predicts the motion of the sabot components. Cui[8] applied a new photographic method by means of the visual light. Plostins[9] proposed the model for planer motion describing the linear and angular motions of a KE penetrator during the sabot discard. The model in nonlinear least square fit was, then, suggested, and used transitional ballistics data. The magnitude, direction, and duration of the sabot discard disturbances are then extracted. Yang,[10] *et al.* studied the asymmetry in the sabot discard process of APFSDS using numerical simulation experiment. A CFD study of the aerodynamic of a sabot separating from a gun-launched projectile was reported by Lesage and Row[11]. Sabot discard aerodynamics was studied both numerically and experimentally by Champigny[12] only at Mach number 3.5 for various orientations and location of sabot wrt the projectile.

In the previous work, the authors studied projectile motion during phase I and phase II. In this paper, the motion in the third phase is discussed in which

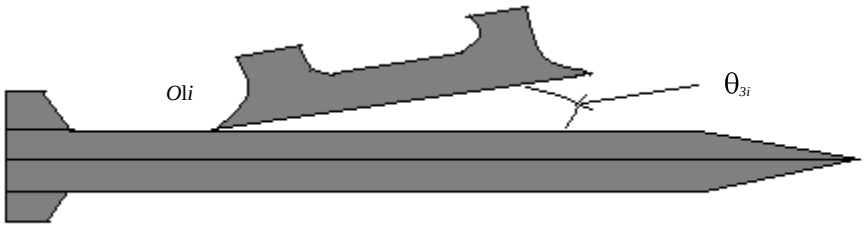

Figure 2. Angle θ_{3i} between the sabot and the projectile.

the stress is on shockwave pressure modelling and its effects on the sabot separation. To analyse the effect of time lag during sabot opening process, the following three cases have been considered:

(i) If all the three sabots are opening simultaneously, it results in to the shockwave force whose resultant on the projectile becomes zero.

(ii) If one sabot is opening with a time lag, the time delay considered in this particular case is such that it starts opening at the instant when the mechanical action of the other two sabots is completed. Here, two sabots experience the shockwave force whereas the third sabot starts its mechanical action.

(iii) If one sabot completes its second phase, and the other two sabots start the opening process, then in this case, the projectile suffers from stability as the modified stability parameter[13] $S > 2$. The shock wave force is expressed as pressure acting on the cross-sectional area of each sabot. The pressure is modelled with the help of free propagating idea[14].

2. SHOCKWAVE PRESSURE MODELLING

The small angle θ_{3i} is developed between the sabot and projectile, which was studied in the second phase (Fig. 1). In the third phase, the air flow enters between projectile body and sabot and shockwave is developed which passes over the sabot towards the tip.

In the general case, for 1-D, unsteady flows, the governing equations are expressed by Whitham[14] are:

$$\left.\begin{aligned} &\frac{\partial \rho}{\partial t}+\rho\frac{\partial u}{\partial x}+u\frac{\partial \rho}{\partial x}=-\frac{\rho u dA}{A dx};\\ &\frac{\partial u}{\partial t}+u\frac{\partial u}{\partial x}+\frac{1}{\rho}\frac{\partial p}{\partial x}=-f\ ;\\ &\frac{\partial s}{\partial t}+u\frac{\partial s}{\partial x}=\frac{uf+q}{T}\ ;\\ &p=p(\rho,s);\end{aligned}\right\} \quad (1)$$

where p, ρ, u are the pressure, density, and flow velocity of gas particle, respectively; s is the entropy, f is the frictional force per unit mass of gas, q is the heat transfer rate per unit mass of gas, T is the temperature of gas, and A is the cross-sectional area.

For an isentropic gas flow, the heat transfer q and friction f are neglected, then

$$\frac{ds}{dt}=0 \quad \text{which gives} \quad \frac{dp}{dt}=a^2\frac{d\rho}{dt} \quad (2)$$

When a moving shock travels through a variable cross-sectional area, the shock itself and the flow behind it are disturbed. The shock strength and the shock front will change which generate some reflected disturbances and nonuniform flow fields behind the shock. While the reflected disturbances move in to the noununiform flow field, the re-reflected disturbances occur, some will overtake the shock and charge its strength and shape also.

In free-propagation concept, the influence of the re-reflected disturbance waves on the shockwave is neglected. Here, this concept is used to get the change in the cross-sectional area due to pressure.

For homentropic flow, some continuous pressure waves are present. In double-wave flows, there are both right traveling and left traveling waves whereas in simple wave flows, one of them is present. The equations

$$u+\frac{2a}{\upsilon-1}=k_1 \quad along \ \frac{dx}{dt}=u+a \quad (3)$$

$$u-\frac{2a}{\upsilon-1}=k_2 \quad along \ \frac{dx}{dt}=u-a \quad (4)$$

represent the right traveling waves, and left traveling waves, respectively. Hence, there are two families of waves or characteristics.

For constant cross-sectional area, the governing equations for isentropic flow become:

$$\left.\begin{aligned}
&\frac{\partial \rho}{\partial t}+\rho\frac{\partial u}{\partial x}+u\frac{\partial \rho}{\partial x}=0 \quad ;\\
&\frac{\partial u}{\partial t}+u\frac{\partial u}{\partial x}+\frac{1}{\rho}\frac{\partial p}{\partial x}=0 \quad ;\\
&\frac{\partial s}{\partial t}+u\frac{\partial s}{\partial x}=0 \quad ;\\
&p=p(\rho,s);
\end{aligned}\right\} \tag{5}$$

From Eqns (2) and (5), one has

$$\frac{1}{\rho a}\frac{\partial p}{\partial t}+\frac{u}{\rho a}\frac{\partial p}{\partial x}+a\frac{\partial u}{\partial x}=0 \tag{6}$$

$$\frac{1}{\rho}\frac{\partial p}{\partial x}+\frac{\partial u}{\partial t}+u\frac{\partial u}{\partial x}=0 \tag{7}$$

By combining Eqns (6) and (7), one gets

$$\left\{\begin{aligned}
&[\frac{\partial u}{\partial t}+(u+a)\frac{\partial u}{\partial x}]+\frac{1}{\rho a}[\frac{\partial p}{\partial t}+(u+a)\frac{\partial p}{\partial x}]=0 \quad (8)\\
&[\frac{\partial u}{\partial t}+(u-a)\frac{\partial u}{\partial x}]+\frac{1}{\rho a}[\frac{\partial p}{\partial t}+(u-a)\frac{\partial p}{\partial x}]=0 \quad (9)\\
&\frac{\partial s}{\partial t}+u\frac{\partial s}{\partial x}=0 \quad (10)
\end{aligned}\right.$$

or

$$\left\{\begin{aligned}
&(\frac{du}{dt})_I+\frac{1}{\rho a}(\frac{dp}{dt})_I=0 \quad (11)\\
&(\frac{du}{dt})_{II}-\frac{1}{\rho a}(\frac{dp}{dt})_{II}=0 \quad (12)\\
&(\frac{ds}{dt})_{III}=0 \quad (13)
\end{aligned}\right.$$

$$\left\{\begin{aligned}
&du+\frac{1}{\rho a}dp=0 \quad along \quad \frac{dx}{dt}=u+a \quad (14)\\
&du-\frac{1}{\rho a}dp=0 \quad along \quad \frac{dx}{dt}=u-a \quad (15)\\
&ds=0 \quad along \quad \frac{dx}{dt}=u \quad (16)
\end{aligned}\right.$$

The three families represent right traveling and left traveling pressure waves and the particle paths, respectively. It means the disturbance of entropy propagates in the flow field with the velocity of gas particle.

With a variable cross-sectional area, the above equations get modified to

$$p+\rho a du+\frac{\rho a^2 u}{u+a}\frac{dA}{A}=0 \ along\ C^+ \quad \frac{dx}{dt}=u+a \tag{17}$$

$$dp-\rho a du+\frac{\rho a^2 u}{u-a}\frac{dA}{A}=0 \ along\ C^- \quad \frac{dx}{dt}=u-a \tag{18}$$

$$ds-a^2 dp=0 \ along\ P \quad \frac{dx}{dt}=u \tag{19}$$

These three families of characteristics in the flow field, that is, characteristics C^+, characteristics C^- and characteristics P are the particle paths Fig. 3. From the physical point of view, the positive characteristics labeled as C^+ have the same direction as the shock-wave; the negative characteristics labeled as C^- are generated by the variable- strength shock. The negative characteristics are the reflected disturbance waves. When the re-reflected disturbance waves are neglected, the positive characteristics only play a subsidiary role. The basic equation along a characteristic

$$p+\rho a du+\frac{\rho a^2 u}{u+a}\frac{dA}{A}=0 \tag{20}$$

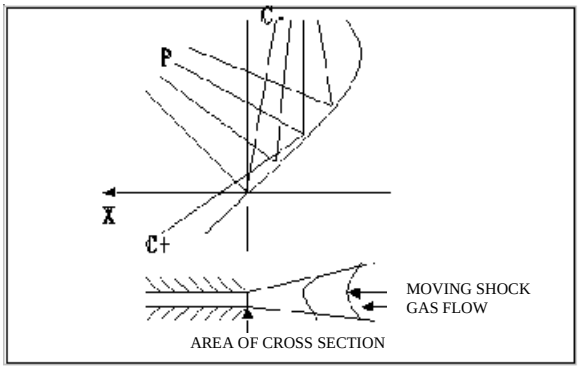

Figure 3. A shockwave moving through a variable cross-sectional area.

The moving shock relations are as follows:

$$\left.\begin{aligned} p_2 &= p_1\left(\frac{2\gamma}{\gamma+1}M^2-\frac{\gamma-1}{\gamma+1}\right)\\ \rho_2 &= \rho_1\frac{(\gamma+1)M^2}{(\gamma-1)M^2+2}\\ u_2 &= \frac{2a_1}{(\gamma+1)}(M-\frac{1}{M})\\ a_2 &= a_1\frac{2\gamma M^2-(\gamma-1)]^{1/2}[(\gamma-1)M^2+2]^{1/2}}{(\gamma+1)M} \end{aligned}\right\} \quad (21)$$

C^+ is given as

from the Eqn (21)

$$dp_2 = P_1\frac{4\gamma}{\gamma+1}MdM \quad (22)$$

$$du_2 = \frac{2a_1}{(\gamma+1)}(1+\frac{1}{M^2})dM \quad (23)$$

$$\rho_2 a_2 = \frac{\rho_1 a_1 M}{\mu} \quad (24)$$

where, $\mu=\left[\frac{(\gamma-1)M^2+2}{2\gamma M^2-(\gamma-1)}\right]^{1/2}$, which represents the Mach numbers for the propagation of a moving shock relative to the flow field behind it.

From the Eqns (20) and (23), one has

$$\frac{\rho_2 a_2 u_2}{u_2+a_2} = \frac{2\rho_1 a_1{}^2\mu(M^2-1)[2\gamma M^2-(\gamma-)]}{[2\mu(M^2-1)+(\gamma-1)M^2+2]} \quad (25)$$

From the Eqns (1), (21), (22), (23), and (24), the relation between the shock Mach number and the cross-sectional area is

$$\frac{2MdM}{(M^2-1)K(M)}+\frac{dA}{A}=0 \quad (26)$$

where

$$K(M)=[2(2\mu+1+M^{-2})^{-1}(1+\frac{2}{\gamma+1}\frac{1-\mu^2}{\mu})^{-1}]$$

Integrating Eqn (26), one has

$$A = C\exp\left[-\int\frac{2MdM}{(M^2-1)K(M)}\right] = Cf(M)$$

where, $C=\frac{A_0}{f(M_0)}$ (27)

$$\frac{A}{A_0}=\frac{f(M)}{f(M_0)} \quad (28)$$

where

$$\begin{aligned} f(M) = \exp\{-\{&\ln(\frac{M^2-1}{M})+\frac{1}{\gamma}\ln(M^2-\frac{\gamma-1}{2\gamma})\\ &+\ln(\frac{1-\mu}{1+\mu})+(\frac{\gamma-1}{2\gamma})^{1/2}\ln[\mu+(\frac{\gamma-1}{2\gamma})^{1/2}]\\ &-(\frac{\gamma-1}{2\gamma})^{1/2}\ln[\mu-(\frac{\gamma-1}{2\gamma})^{1/2}]+[\frac{2}{\gamma(\gamma-1)}]^{1/2}\\ &\ln[(M^2+\frac{2}{\gamma-1})^{1/2}+(M^2-\frac{\gamma-1}{2\gamma})^{1/2}]+[\frac{1}{2(\gamma-1)}]^{1/2}\\ &\tan^{-1}\{\frac{[4\gamma-(\gamma-1)]M^2-4(\gamma-1)}{4\gamma^{1/2}(\gamma-1)[M^2+\frac{2}{\gamma-1}]^{1/2}[M^2-\frac{\gamma-1}{2\gamma}]^{1/2}}\}\}\} \end{aligned}$$

Suffix 0 denotes the initial condition for this motion which is the same as the final condition for phase II.

3. EQUATIONS OF MOTION OF PROJECTILE

3.1 Forces

The propellant gas force, aerodynamic force, and gravity force acting on the projectile[2] are similar to those in phase II. The additional forces due to the sabot opening process are discussed here

3.1.1 Model for the Shockwave Force F4

The shockwave force is obtained by assuming the shockwave pressure acting on the cross-sectional area of the sabot.

A shockwave force for each sabot component is given by

$$\begin{aligned}\bar{F}_4 &= \text{Shockwave force} \\ &= -\text{Pressure x Area of cross section of sabot x } \hat{i}_{3i}\end{aligned} \quad (29)$$

$$\bar{F}_4 = \sum \bar{F}_{4i} = \text{Shockwave force}$$

From the Eqn (22), the pressure due to shock is given by

$$p_2 = p_1\left(\frac{2\gamma}{\gamma+1}M^2 - \frac{\gamma-1}{\gamma+1}\right)$$

$$\bar{F}_4 = -p_1\left(\frac{2\gamma}{\gamma+1}M^2 - \frac{\gamma-1}{\gamma+1}\right)\pi(D_s{}^2/4)\hat{i}_{3i} \quad (30)$$

$$= -p_1\left(\frac{2\gamma}{\gamma+1}M^2 - \frac{\gamma-1}{\gamma+1}\right)\pi(D_s{}^2/4)(\cos\theta_{3i}\hat{i}_{1i} + \sin\theta_{3i}\hat{j}_{1i})$$

$$\therefore \bar{F}_4 = \Sigma \bar{F}_{4i}$$

$$= \sum_{i=1}^{3} -p_1\left(\frac{2\gamma}{\gamma+1}M^2 - \frac{\gamma-1}{\gamma+1}\right)\pi(D_s{}^2/4)(\cos\theta_{3i}\hat{i}_{1i} + \sin\theta_{3i}\hat{j}_{1i})$$

$$= -p_1\left(\frac{2\gamma}{\gamma+1}M^2 - \frac{\gamma-1}{\gamma+1}\right)\pi(D_s{}^2/4)\sum_{i=1}^{3}(\cos\theta_{3i}\hat{i}_{1i} + \sin\theta_{3i}\hat{j}_{1i}) \quad (31)$$

3.1.2 Shockwave Moment

In the phase III, the mechanical force is absent, thus the mechanical action moment is zero and shockwave force generates the corresponding moment:

$$\bar{M}_{c4} = \bar{r}_1 \; X \; \bar{F}_4 \quad (32)$$

$$\begin{aligned}\bar{M}_{c4} &= \text{Shockwave force moment} \\ &= \text{Distance X Force} \\ &= \overline{O_{1i}C} \; X \; \bar{F}_4 \\ &= \bar{r}_1 \; X \sum_{i=1}^{3}\bar{F}_4 = r_1\hat{i}_1 \; X \sum_{i=1}^{3}\bar{F}_{4i} \quad [\text{But } \hat{i}_1 = \hat{i}_1] \\ &= [r\hat{i}_1] X \; [-p_1\left(\frac{2\gamma}{\gamma+1}M^2 - \frac{\gamma-1}{\gamma+1}\right) \\ &\quad \pi\,(D_s{}^2/4)\cos\theta_{3i}\;\hat{i}_1]\end{aligned} \quad (33)$$

$$\therefore \; \bar{M}_{c4} = 0 \qquad [\because \; \hat{i}_1 \; X \; \hat{i}_1 = 0] \quad (34)$$

3.2 6-DOFs Equations for Projectile

In the third phase of motion, the trajectory of the projectile in 6-DOFs can be obtained with the remaining four forces except mechanical force. The force and moment equations are resolved in velocity and projectile coordinate system respectively (Fig. 4). The scalar equations are

Force equations

$$\begin{aligned}\dot{V}_P = \{&PA[(\cos\varepsilon_1\cos\varepsilon_2\cos\theta_2\cos\phi_2 - \sin\varepsilon_1\cos\varepsilon_2\sin\theta_2 \\ &-\sin\varepsilon_2\cos\theta_2\sin\phi_2) + (1/2)\rho S V_p{}^2\{-C_D + \\ &(l/V_P)C_{Nqt}[\sin\delta_1(-\dot{\phi}_1\sin\gamma_1\cos\theta_1 + \dot{\theta}_1\cos\gamma_1) \\ &+\cos\delta_1\sin\delta_2(\dot{\phi}_1\cos\gamma_1\cos\theta_1 + \dot{\theta}_1\sin\gamma_1)]\} \\ &-p_1\left(\frac{2\gamma}{\gamma+1}M^2 - \frac{\gamma-1}{\gamma+1}\right)\pi\,(D_s{}^2/4) \\ &\cos\theta_{3i}\cos\delta_1\cos\delta_2 - mg\sin\theta_2\}/m\end{aligned} \quad (35)$$

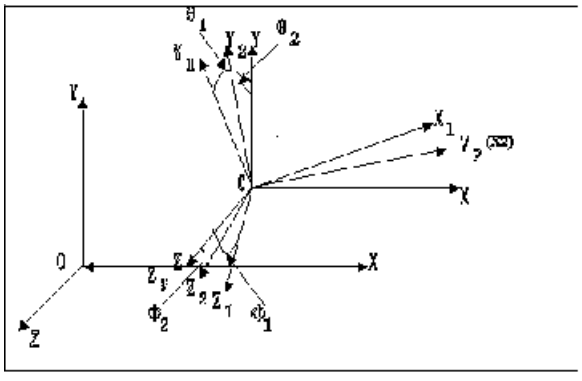

Figure 4. Angle of side slips, angle of attack and velocity.

$$\dot{\phi}_2 = \{PA(\cos\varepsilon_1\cos\varepsilon_2\sin\phi_2 + \sin\varepsilon_2\cos\phi_2) + (1/2)\rho SV_p^{\,2}\{[-C_{L\alpha}\sin\delta_1\cos\delta_2 - (pl/V_p)C_{Np\alpha}\sin\delta_2 + (l/V_P)C_{Nqt}[\cos\delta_1(-\dot{\phi}_1\sin\gamma_1\cos\theta_1 + \dot{\theta}_1\cos\gamma_1) - \sin\delta_1\sin\delta_2(\dot{\phi}_1\cos\gamma_1\cos\theta_1 + \dot{\theta}_1\sin\gamma_1)]\} + p_1\left(\frac{2\gamma}{\gamma+1}M^2 - \frac{\gamma-1}{\gamma+1}\right)\pi\,(\mathrm{D_s}^2/4)\cos\theta_{3i}\sin\delta_1\cos\delta_2\}/(-mV_P\dot{\phi}_2\cos\theta_2) \tag{36}$$

$$\dot{\theta}_2 = \{PA(\cos\varepsilon_1\cos\varepsilon_2\sin\theta_2\cos\phi_2 + \sin\varepsilon_1\cos\varepsilon_2\cos\theta_2 - \sin\varepsilon_2\sin\theta_2\sin\phi_2) + (1/2)\rho SV_p^{\,2}[C_{L\alpha}\sin\delta_2 - (pl/V_p)C_{Np\alpha}\sin\delta_1\cos\delta_2 - (l/V_P)C_{Nqt}\cos\delta_2(\dot{\phi}_1\cos\gamma_1\cos\theta_1 + \dot{\theta}_1\sin\gamma_1)] - p_1\left(\frac{2\gamma}{\gamma+1}M^2 - \frac{\gamma-1}{\gamma+1}\right)\pi\,(\mathrm{D_s}^2/4)\cos\theta_{3i}\sin\delta_2 + mg\cos\theta_2\}/(-mV_P) \tag{37}$$

Moment equations

$$I_{xx}(\partial/\partial t)(\dot{\phi}_1\sin\theta_1 + \dot{\gamma}_1) = r_p PA(-\sin\eta_1\cos\eta_2\sin\varepsilon_2 + \sin\eta_2\sin\varepsilon_1\cos\varepsilon_2) + (1/2)\rho\,SV_p^{\,2}l\,\mathrm{C_{tp}}(pl/V_p) \tag{38}$$

$$\begin{aligned} &I_{YY}(\partial/\partial t)(\dot{\phi}_1\cos\gamma_1\cos\theta_1 + \dot{\theta}_1\sin\gamma_1) \\ &= +(I_{YY} - I_{xx})(\dot{\phi}_1\sin\theta_1 + \dot{\gamma}_1)(-\dot{\phi}_1\sin\gamma_1\cos\theta_1 + \dot{\theta}_1\cos\gamma_1)] \\ &+ r_p PA(\sin\eta_2\cos\varepsilon_1\ \cos\varepsilon_2 - \cos\eta_1\cos\eta_2\sin\varepsilon_2) + (1/2)\rho\,SV_p^{\,2}l[-\mathrm{C_{M\alpha}}\cos\delta_1\sin\delta_2 \\ &+ \mathrm{C_{M\alpha p}}(pl/V_p)\sin\delta_1 + (l/V_P)(\mathrm{C_{Mqt}})(\dot{\phi}_1\cos\gamma_1\cos\theta_1 + \dot{\theta}_1\sin\gamma_1)] \end{aligned} \tag{39}$$

$$\begin{aligned} &[I_{YY}(\partial/\partial t)(-\dot{\phi}_1\sin\gamma_1\cos\theta_1 + \dot{\theta}_1\cos\gamma_1) + (I_{YY} - I_{xx})(\dot{\phi}_1\sin\theta_1 + \dot{\gamma}_1)(\dot{\phi}_1\cos\gamma_1\cos\theta_1 + \dot{\theta}_1\sin\gamma_1)] \\ &= r_p PA(-\cos\eta_1\cos\eta_2\sin\varepsilon_1\cos\varepsilon_2 + \sin\eta_1\cos\eta_2\cos\varepsilon_1\ \cos\varepsilon_2) + (1/2)\rho\,SV_p^{\,2}l[-\mathrm{C_{M\alpha}}\sin\delta_1 \\ &+ \mathrm{C_{M\alpha p}}(pl/V_p)\cos\delta_1\sin\delta_2 + (l/V_P)(\mathrm{C_{Mqt}})(-\dot{\phi}_1\sin\gamma_1\cos\theta_1 + \dot{\theta}_1\cos\gamma_1)] \end{aligned} \tag{40}$$

The velocity in inertial frame is

$$\dot{x} = V\cos\theta_2\cos\phi_2 \tag{41}$$

$$\dot{y} = V\sin\theta_2\cos\phi_2 \tag{42}$$

$$\dot{z} = -V\sin\phi_2 \tag{43}$$

3.3 Equations of Motion for Sabot Components

The sabot components move relative to the projectile body. Here, the influence factor involves shock wave action along with the propellant gas force. The motion equations of each sabot component will be established in the projectile-fixed coordinate system.

The force equations of the sabot are resolved in projectile-fixed coordinate system. Different forces are:

$$\bar{F}_s = \{PA\cos\eta_1\cos\eta_2 + (1/2)\rho S_s u^2 C_{xs} - p_1\left(\frac{2\gamma}{\gamma+1}M^2 - \frac{\gamma-1}{\gamma+1}\right)\pi(Ds/2)Ls - m_s g\sin\theta_1\}\hat{i}_{1i}$$
$$+\{-PA(\sin\eta_1\cos\eta_2\cos\gamma_i + \sin\eta_2\sin\gamma_i) + (1/2)\rho S_s u^2(l_s/u)C_{Nqs}(\dot{\theta}_1\cos\gamma_i + \dot{\phi}_1\cos\theta_1\sin\gamma_i) - m_s g\cos\gamma_{1i}\cos\theta_1\}\hat{j}_{1i}$$
$$+\{PA(-\sin\eta_1\cos\eta_2\sin\gamma_i + \sin\eta_2\cos\gamma_i) + (1/2)\rho S_s u^2(l_s/u)C_{Nqs}(\dot{\theta}_1\sin\gamma_i - \dot{\phi}_1\cos\theta_1\cos\gamma_i) + m_s g\sin\gamma_i\cos\theta_1\}\hat{k}_{1i} \quad (44)$$

The dynamic vector equations of the centre motion of all sabot components are obtained

$$m(\bar{a}_{ir} + \bar{a}_{ie} + \bar{a}_{ik}) = \sum\bar{F}_s = \bar{F}_{1s} + \bar{F}_{2s} + \bar{F}_{3s} + \bar{F}_{4s} + \bar{F}_{5s} \quad (45)$$

Total acceleration of the i[th] sabot is similar to the phase II[2].

The relative scaler equations of the sabot are:

$$\begin{aligned} &PA\cos\eta_1\cos\eta_2 + (1/2)\rho S_s u^2 C_{xs} - p_1\left(\frac{2\gamma}{\gamma+1}M^2 - \frac{\gamma-1}{\gamma+1}\right)\pi(Ds/2)Ls - m_s g\sin\theta_1 \\ &= -L_c[\ddot{\theta}_{3i}\sin\theta_{3i} + (\dot{\theta}_{3i})^2\cos\theta_{3i}] + \dot{V}_p\cos\delta_1\cos\delta_2 - \frac{\partial\dot{\theta}_1}{\partial t}(L_c\sin\theta_{3i} + \frac{l}{2}) \\ &+ (\dot{\gamma}_1\dot{\phi}_1\cos\theta_1 + \dot{\phi}_1^2\cos\theta_1\sin\theta_1)(L_c\sin\theta_{3i} + \frac{l}{2}) \\ &- \dot{\phi}_1^2\cos^2\theta_1\ (L_c\cos\theta_{3i} - L_m)\ - \dot{\theta}_1^2(L_c\cos\theta_{3i} - L_m) \end{aligned} \quad (46)$$

$$\begin{aligned} &-PA(\sin\eta_1\cos\eta_2\cos\gamma_i + \sin\eta_2\sin\gamma_i) + (1/2)\rho S_s u^2(l_s/u)C_{Nqs}\ (\dot{\theta}_1\cos\gamma_i + \dot{\phi}_1\cos\theta_1\sin\gamma_i) - m_s g\cos\gamma_{1i}\cos\theta_1 \\ &= L_c[\ddot{\theta}_{3i}\cos\theta_{3i} - (\dot{\theta}_{3i})^2\sin\theta_{3i}] + \dot{V}_p(\sin\delta_1\cos\gamma_i + \cos\delta_1\sin\delta_2\sin\gamma_i) + \frac{\partial\dot{\theta}_1}{\partial t}(L_c\cos\theta_{3i} - L_m) - \dot{\theta}_1^2(L_c\sin\theta_{3i} + \frac{l}{2}) \\ &- (\dot{\gamma}_1 + \dot{\phi}_1\sin\theta_1)^2(L_c\sin\theta_{3i} + \frac{l}{2}) + (\dot{\gamma}_1 + \dot{\phi}_1\sin\theta_1)\dot{\phi}_1\cos\theta_1(L_c\cos\theta_{3i} - L_m) \end{aligned} \quad (47)$$

$$\begin{aligned} &PA(-\sin\eta_1\cos\eta_2\sin\gamma_i + \sin\eta_2\cos\gamma_i) + (1/2)\rho S_s u^2(l_s/u)C_{Nqs}(\dot{\theta}_1\sin\gamma_i - \dot{\phi}_1\cos\theta_1\cos\gamma_i) + m_s g\sin\gamma_i\cos\theta_1 \\ &= \dot{V}_p(\sin\delta_1\sin\gamma_i - \cos\delta_1\sin\delta_2\cos\gamma_i) + \frac{\partial(\dot{\gamma}_1 + \dot{\phi}_1\sin\theta_1)}{\partial t}(L_c\sin\theta_{3i} + \frac{l}{2}) + \frac{\partial(\dot{\phi}_1\cos\theta_1)}{\partial t}(L_c\cos\theta_{3i} - L_m) \\ &+ \dot{\theta}_1(\dot{\gamma}_1 + \dot{\phi}_1\sin\theta_1)(L_c\cos\theta_{3i} - L_m) + \dot{\phi}_1\dot{\theta}_1\cos\theta_1(L_c\sin\theta_{3i} + \frac{l}{2}) \end{aligned} \quad (48)$$

3.4 Moment Equations of Sabot

Above forces generate moments due to which sabots move relative to projectile. The relative moment equations of sabot component relative to projectile are:

$$\begin{aligned} &I_{XXS}\frac{\partial}{\partial t}(\dot{\gamma}_1 + \dot{\phi}_1\sin\theta_1) + \dot{\phi}_1\cos\theta_1(I_{ZZS}(\dot{\theta}_1 + \dot{\theta}_{3i}) - \dot{\theta}_1 I_{YYS}) \\ &= L_C PA\sin\theta_{3i}(-\sin\eta_1\cos\eta_2\sin\gamma_i + \sin\eta_2\cos\gamma_i) + Ms\{[V_c(\sin\delta_1\cos\gamma_i + \cos\delta_1\sin\delta_2\sin\gamma_i) \\ &+ \dot{\theta}_1 L_m(\dot{\theta}_1 + \dot{\theta}_{3i})L_c\cos\theta_{3i}][V_c(\sin\delta_1\sin\gamma_i - \cos\delta_1\sin\delta_2\cos\gamma_i) \end{aligned}$$

$$+\frac{l}{2}(\dot{\gamma}_1+\dot{\phi}_1\sin\theta_1)+\dot{\phi}_1\cos\theta_1 L_m]-m[V_c(\sin\delta_1\sin\gamma_i-\cos\delta_1\sin\delta_2\cos\gamma_i)+\frac{l}{2}(\dot{\gamma}_1+\dot{\phi}_1\sin\theta_1)$$
$$+\dot{\phi}_1\cos\theta_1 L_m+(\dot{\gamma}_1+\dot{\phi}_1\sin\theta_1)L_c\sin\theta_{3i}-\dot{\phi}_1\cos\theta_1 L_c\cos\theta_{3i}][V_c(\sin\delta_1\cos\gamma_i+\cos\delta_1\sin\delta_2\sin\gamma_i)+\dot{\theta}_1 L_m] \quad (49)$$

$$I_{YYS}\frac{\partial}{\partial t}(\dot{\phi}_1\cos\theta_1)+(\dot{\gamma}_1+\dot{\phi}_1\sin\theta_1)[\dot{\theta}_1 I_{XXS}-I_{ZZS}(\dot{\theta}_1+\dot{\theta}_{3i})]$$
$$=-L_C PA\cos\theta_{3i}(-\sin\eta_1\cos\eta_2\sin\gamma_i+\sin\eta_2\cos\gamma_i)+(1/2)\rho S_s V^2 l_s\{C_{M\rho\alpha s}(\sin\delta_1\cos\gamma_i-\cos\delta_1\sin\delta_2\sin\gamma_i)]$$
$$+Ms[V_c(\sin\delta_1\sin\gamma_i-\cos\delta_1\sin\delta_2\cos\gamma_i)+\frac{l}{2}(\dot{\gamma}_1+\dot{\phi}_1\sin\theta_1)+\dot{\phi}_1\cos\theta_1 L_m+(\dot{\gamma}_1+\dot{\phi}_1\sin\theta_1)L_c\sin\theta_{3i}$$
$$-\dot{\phi}_1\cos\theta_1 L_c\cos\theta_{3i}][V_c\cos\delta_1\cos\delta_2-\frac{l}{2}\dot{\theta}_1]-Ms[V_c\cos\delta_1\cos\delta_2-\frac{l}{2}\dot{\theta}_1-(\dot{\theta}_1+\dot{\theta}_{3i})L_c\sin\theta_{3i}] \quad (50)$$
$$[V_c(\sin\delta_1\sin\gamma_i-\cos\delta_1\sin\delta_2\cos\gamma_i)+\frac{l}{2}(\dot{\gamma}_1+\dot{\phi}_1\sin\theta_1)+\dot{\phi}_1\cos\theta_1 L_m]$$

$$I_{ZZS}\frac{\partial}{\partial t}(\dot{\theta}_1+\dot{\theta}_{3i})+I_{YYS}\dot{\phi}_1\cos\theta_1(\dot{\gamma}_1+\dot{\phi}_1\sin\theta_1-\dot{\phi}_1\cos\theta_1)$$
$$=-[L_C PA\cos\theta_{3i}(\sin\eta_1\cos\eta_2\cos\gamma_i+\sin\eta_2\sin\gamma_i)+L_C PA\sin\theta_{3i}\cos\eta_1\cos\eta_2]+(1/2)\rho S_s V^2 l_s[C_{M\rho\alpha s}(\sin\delta_1\sin\gamma_i$$
$$+\cos\delta_1\sin\delta_2\cos\gamma_i)+(l_s/V)C_{Mqs}\dot{\theta}_{3i}]+Ms[V_c\cos\delta_1\cos\delta_2-\frac{l}{2}\dot{\theta}_1-(\dot{\theta}_1+\dot{\theta}_{3i})L_c\sin\theta_{3i}]$$
$$[V_c(\sin\delta_1\cos\gamma_i+\cos\delta_1\sin\delta_2\sin\gamma_i)+\dot{\theta}_1 L_m]-Ms[V_c(\sin\delta_1\cos\gamma_i+\cos\delta_1\sin\delta_2\sin\gamma_i)$$
$$+\dot{\theta}_1 L_m(\dot{\theta}_1+\dot{\theta}_{3i})L_c\cos\theta_{3i}][V_c\cos\delta_1\cos\delta_2-\frac{l}{2}\dot{\theta}_1] \quad (51)$$

3.5 Simulation Results

Initial values of the variables *t, V, x, y, z,* Φ_1, Φ_2, θ_1, θ_2, γ_1, θ_3, and $\theta_3$dot of this phase are the end results of phase II[2]. Interval for phase III is taken to be 0.002 to 0.003 s.

The motion has been simulated for the following data with fixed step size h=0.0001. This is given in Table 1.

The maximum stretch of the spring is assumed to be 5.089E-05 mm. This gives the maximum cross sectional area (Table 2) beyond which the effect of sabot over the projectile is nullified.

In this time interval of 0.001 s, it is observed that the projectile travels a distance of 1.447 m (Fig. 5), velocity decreases by approximate 2.1 m/s (Fig. 6). Angle of attack θ_2 decreases but θ_1 remains constant. Angles of side slip Φ_2 and Φ_1 increases. Angle θ_{3i} between sabot and projectile starts increasing and it increases by 1.3985° (Fig.7).

- The velocity of the projectile and hence the Mach number decreases for the projectile due to air resistance.
- Due to the air flow between the sabot and the projectile, it is observed that the pressure at the tip of sabot increases from 46.112 MPa to 987.2429 MPa and then starts decreasing. Area of cross section increases (Fig. 8). The area increases till the maximum stretch of the spring due to the sabot gets totally separated from the projectile.
- The pressure beyond the tip of sabot decreases.

3.6 Data

P = 46.112 MPa	I_{xx} = 3.66 kg/m^3	? = 1.225 kg/m^3	I_{yy} = 549.06 kg/m^3
I = 0.486 m	m = 6.4 kg	p = 145 rpm	C_x = 1.25
C_N = 7.02	C_{Npa} = 0	C_{Nqa} = 0	C_{tp} = 0
C_{Mqt} = -570.6	C_{Nq} = 0	V_P = 1445.8 m/s	$C_{M\alpha}$ = 2.5
F $_2$ = 0.0346285^0	?$_2$ = 0.0659733	F $_1$ = 1.1992171^0	F $_1$dot = 0.03066^0
θ_1 = 1.5^0	?$_1$dot = –0.3942^0	?$_3$ = 1.480331^0	?$_3$dot = 1.5803565^0
γ_1 = 0.5^0	x = 2.8957	y = 0.004322	z = –0.0007694
? 1 = ?2 = e1 = e2 = ?1 = 0		t = 0.001 s	Ds = 0.066 m
?$_s$ = 71.2 m	Lc = 0.3 m	Ls = 0.4 m	Lm = 0.346 m
m_s = 2.8	I_{xxs} = 0.4 kg/m^3	I_{yys} = 50.4 kg/m^3 = I_{zzs}	C_{mps} = –2.6
C_{mqs} = –58	k = 1.25	px = 1.67 g/cm^3	U = 1445.8
X = 347.3	d = 0.104 m	? = 1.25	a = 340 m/s

Table 1. Trajectory of the projectile in phase III

t	*V*	*x*	*y*	*z*
0.002	1445.8	2.8957	0.004323	–0.0007705
0.0021	1445.6	3.0403	0.0044868	–0.00085998
0.0022	1445.4	3.1848	0.0046449	–0.00095401
0.0023	1445.2	3.3293	0.0047974	–0.0010526
0.0024	1445	3.4738	0.0049473	–0.00115557
0.0025	1444.7	3.6183	0.0050856	–0.0012633
0.0026	1444.5	3.7628	0.0052212	–0.0013755
0.0027	1444.3	3.9072	0.0053512	–0.0014922
0.0028	1444.1	4.0517	0.0054755	–0.0016134
0.0029	1443.9	4.1961	0.0055942	–0.0017392
0.0030	1443.7	4.3404	0.0057072	–0.0018694

	?$_2$ deg	**? $_1$ deg**	**?$_1$deg**	**?$_1$deg**	**?$_3$dot deg**	**?$_3$ deg**
0.034557	0.065996	1.1917	1.5004	0.50055	1.5798	1.4797
0.036363	0.063785	1.1908	1.5003	0.50058	1.7188	1.6187
0.038166	0.061568	1.1899	1.5003	0.50061	1.858	1.7579
0.039968	0.059345	1.189	1.5002	0.50065	1.9974	1.8973
0.041768	0.057123	1.1882	1.5002	0.50068	2.137	2.0369
0.043566	0.054897	1.1873	1.5002	0.5007	2.2767	2.1766
0.045363	0.052669	1.1863	1.5001	0.50073	2.4166	2.3166
0.047159	0.050437	1.1855	1.5001	0.50077	2.5568	2.4567
0.048952	0.048202	1.1846	1.5001	0.5008	2.6971	2.597
0.050744	0.045964	1.1836	1.5000	0.50082	2.8376	2.7375
0.052535	0.043724	1.1828	1.5000	0.50085	2.9783	2.8782

4. STABILITY OF MOTION

The modified stability parameter has been discussed due to shockwave exerted on the projectile body. The equations for stability in projectile-fixed frame are the same as those in phase II[2]. The changed values of K_i (i=1,2,3,4,5,6) modified the stability parameter[13].

$$S = 1 + \frac{(2K_4 / K_1) - K_2}{\sqrt{K_1^{\,2} + K_2^{\,2}}} \qquad (52)$$

Table 2. Shockwave pressure and area of cross-section at the tip of the sabot

t	*V*	*M*	*μ*	*f* (*M*)	*A*	P_2
0.0020	1445.8	4.258529	0.38067373	8.07343E-06	5.038E-05	987.24285
0.0021	1445.6	4.257941	0.38069012	8.08114E-06	5.043E-05	986.9701
0.0022	1445.4	4.257353	0.380706517	8.08885E-06	5.047E-05	986.69739
0.0023	1445.2	4.256765	0.380722919	8.09658E-06	5.052E-05	986.42471
0.0024	1445.0	4.255882	0.380747535	8.10818E-06	5.059E-05	986.01577
0.0025	1444.7	4.255294	0.380763953	8.11592E-06	5.064E-05	985.74319
0.0026	1444.5	4.254706	0.380780377	8.12367E-06	5.069E-05	985.47065
0.0027	1444.3	4.254118	0.380796807	8.13143E-06	5.074E-05	985.19815
0.0028	1444.1	4.253529	0.380813244	8.1392E-06	5.079E-05	984.92568
0.0029	1443.9	4.252941	0.380829686	8.14697E-06	5.084E-05	984.65325
0.0030	1443.7	4.252353	0.380841346	8.15475E-06	5.089E-05	984.38086

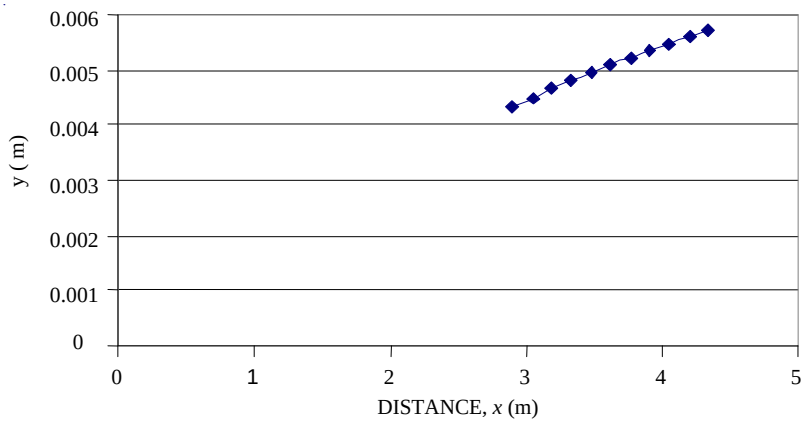

Figure 5. Trajectory in the phase III.

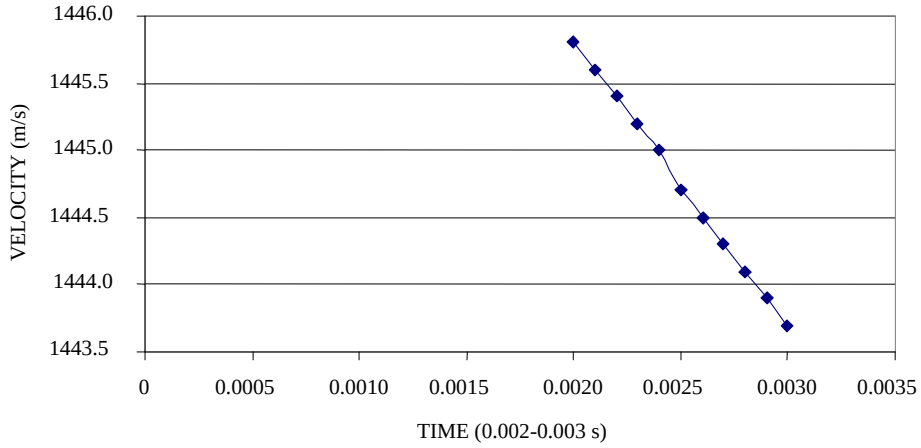

Figure 6. Reduction in the velocity in phase III.

Three particular cases are discussed:

(i) If all the three sabots are opening simultaneously in the phase III, it has been observed that the modified stability parameter is s = 1.841251246.

(ii) One sabot is opening with a time lag. The time delay considered in this particular case is such that it starts opening at the instant when the mechanical action of the other two sabots is completed. In this case, the stability parameter

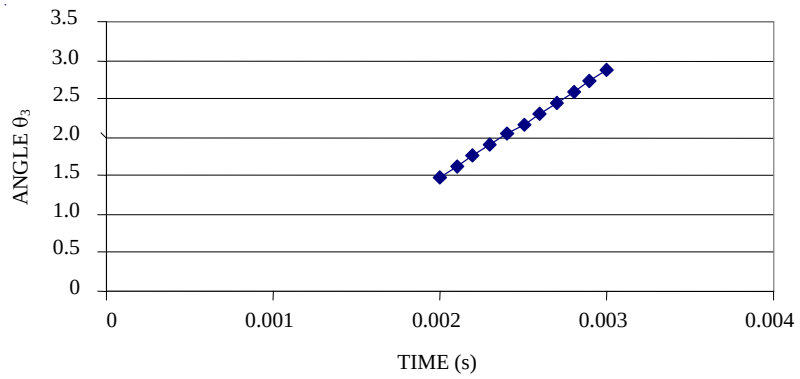

Figure 7. Angle between the sabot and projectile.

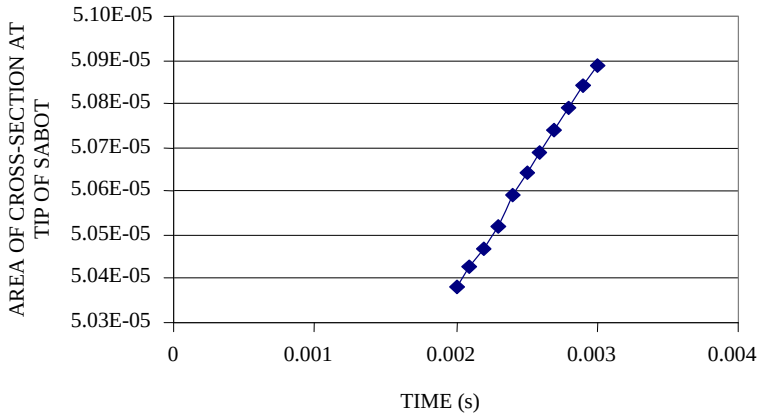

Figure 8. Increase in the area between the sabot and the projectile.

gets modified from S = 1.841251246 to S = 1.994028368.

(iii) One sabot completes its second phase and; the other two sabots start the opening process. In this case, the stability parameter becomes S = 2.197507407 which makes projectile unstable.

5. CONCLUSIONS

- For a FSAPDS projectile, a mathematical model has been developed in third phase where the shockwave force acts on the projectile due to sabot separation. The trajectory has been simulated. It is observed that shockwave force in the simulation does not affect the trajectory of the projectile till the sabots are totally separated from the projectile.

- The modified stability parameter increases due to separation of the sabots but the projectile still remains in phase III.

- The stability of the projectile gets affected due to separation of the sabots with time delay. The projectile may become unstable if the time delay is significant.

ACKNOWLEDGMENTS

The authors are grateful to the Vice Chancellor of the Defence Institute of Advanced Technology (DIAT), Pune, and the Chairman and Director of the P.E. Society's Modern College of Engineering, Pune, for their support and encouragement.

REFERENCES

1. Yang, P. A study on dynamic modeling of sabot discard. Ballistics Research Laboratory, East China Institute of Technology, China. pp. 267-78

2 Acharya, R.S. & Naik, S.D. Perturbation of initial stability of a FSAPDS projectile. *Def. Sci. J.*, 2006, **56**(5), 753-68.

3. Acharya, R.S. & Naik, S.D. Motion analysis during sabot opening process. *Def. Sci. J.*, 2007, **57**(2), 229-41.

4. Gallagher, W.J. Elements which have contributed to dispersion in the 90/40 mm projectile. Ballistics Research Laboratory, Aberdeen Proving Ground, MD, USA, March 1957. Report No. BRL-1013,

5. Conn, H. The influence of sabot separation on the yawing motion of a cone. Defense Research Establishment, Valcartier, Canada, June 1970. Report No. TN 1849/70.

6. Schmist, E.M. & Shear, D.D. Aerodynamic interference during sabot discard. *J. Spacecraft Rockets*, May-June 1978, **15**(3), 162-67.

7. Siegelman, D. & Crimi, P. *In* 5th International Symposium of Ballistics, Vol. 2, 16-18 April 1980. pp. 428-34,

8. Cui, D.; He, Z; Jianguo, G.; Guan, X. & Lea, D. A new method of monitoring sabot discard process in near muzzle region. *In* 12th International Symposium of Ballistics, Vol. 2, 30 October 1990. pp. 240-50.

9. Plastins, P. A method for extracting the sabot discard impulse from transitional ballistics data. *In* 12th International Symposium of Ballistics, San Antonis, Texas, Vol. 2, 30 October 1990, pp. 240-50.

10. Yang, Q.; Xu. Z.; Ru, X. & Xu, M. A study about the asymmetry in the sabot discard process of APFSDS. *In* 13th International Symposium of Ballistics, Vol. 2, 1-3 June 1992. pp.17-24.

11. Lesage, F. & Row, M.G. Navier-Stokes computation of the aerodynamics of symmetric sabot separation. *In* 13th International Symposium of Ballistics, Vol. 2, 1-3 June 1992. pp. 9-16.

12. Champigny, P.; Espiney, P.D. & Ceroni, D. Computation of saboty discard using chimera technique. *In* 17th International Symposium of Ballistics, Vol. 2, 23-27 March 1998.

13. Naik, S.D. Stability criterion for a finned spinning projectile. *Def. Sci. J.*, 2000, **50**, 31-35.

14. Han Z. & Yin, X. Shock dynamics. Kluwer, Academic Publishers–Dordrecht/ Bosten/ London, Hefei, Anhui, P.R. China, 1992. pp. 30-33.